# Size dependence of photoluminescence quantum efficiency of Si nanocrystals

Satoru Miura, Toshihiro Nakamura, Minoru Fujii,* Masaki Inui, and Shinji Hayashi
*Department of Electrical and Electronics Engineering, Faculty of Engineering, Kobe University, Rokkodai, Nada, Kobe 657-8501, Japan*
(Received 15 February 2006; revised manuscript received 17 May 2006; published 26 June 2006)

The radiative recombination rate of excitons confined in Si nanocrystals was modified by placing a Au layer nearby. Oscillation of the rate was observed when the distance between the active layer and the Au layer was changed. By comparing the experimentally obtained oscillation behavior with a calculated one, the radiative and nonradiative recombination rates, and also the internal quantum efficiency of excitons in Si nanocrystals were estimated. The relation between the radiative rate and the luminescence wavelength was on a single curve for all the samples studied. On the other hand, the nonradiative rate depended strongly on samples. For the samples annealed at 1250 °C, the estimated quantum efficiency was close to 100% at longer wavelength side of the luminescence bands, while the maximum quantum efficiency was 70% for the sample annealed at 1200 °C. The present results provide evidence that in Si nanocrystal assemblies, the majority of nanocrystals in samples do not contribute to photoluminescence and a small part of nanocrystals luminesce with high quantum efficiencies, and thus the total quantum efficiency is mainly determined by the number ratio of bright and dark Si nanocrystals in the assembly.

DOI: 10.1103/PhysRevB.73.245333 PACS number(s): 78.67.Bf, 78.55.−m, 78.40.Fy

## I. INTRODUCTION

Silicon nanocrystals (Si-nc's) show strong visible and near-infrared (NIR) photoluminescence (PL) at room temperature due to the recombination of excitons confined in the zero-dimensional quantum confined system.[1–4] The PL external quantum efficiency is usually reported to be several percent.[5–7] The internal quantum efficiency is estimated to be about twice that of the external quantum efficiency in the case of Si-nc's embedded in $SiO_2$ thin films on Si substrates.[7] If the substrate is $SiO_2$, the light extraction efficiency is expected to be larger. The quantum efficiency has been estimated experimentally for an assembly of Si-nc's, and thus those of individual Si-nc's constructing the assembly are not known. Two extreme scenarios are considered as to how the experimentally obtained total quantum efficiency is determined. One scenario is that each nanocrystal constructing the assembly has the same quantum efficiency. The other one is that a small number of nanocrystals have large quantum efficiencies close to 100% and the majority of nanocrystals do not contribute to PL, resulting in a rather low total quantum efficiency. A scenario in-between two extreme cases is also possible. Up to now, the second scenario has widely been accepted, although the studies on this problem are very limited.

Very recently, Kalkman *et al.*[8] and Walters *et al.*[9] demonstrated that the radiative and nonradiative recombination rates of excitons in Si-nc's can be estimated independently by studying the relation between the photonic mode density (PMD) at the position of Si-nc's assemblies and the PL decay rates. They changed the PMD by simply controlling the distance between Si-nc's and a Si substrate, and observed the oscillation of the PL decay rates.[9] By comparing the oscillation behavior with the oscillation of a calculated PMD, they estimated the radiative and nonradiative recombination rates, and also the internal quantum efficiency. The obtained quantum efficiencies were about 80% and were slightly dependent on the wavelength. In this method, quantum efficiencies of Si-nc's contributing to PL in an assembly are extracted. The rather large quantum efficiency means that the second scenario is in principle correct, although the quantum efficiency of "bright" Si-nc's is not 100%.

Although the work revealed important aspects of PL properties of Si-nc assemblies, there remain problems to be clarified. The first one is the origin of nonradiative recombination processes, which make the quantum efficiency of bright Si-nc's to be less than 100%. In their work, Si-nc samples were prepared by an ion-implantation method. Similar samples can be prepared by thermal annealing of $SiO_x$ films deposited by CVD,[10,11] sputtering,[2,12] or vacuum evaporation.[13,14] It is of great interest to compare the results with those obtained for Si-nc samples prepared by other methods and to study whether the values are common for Si-nc's or specific for their samples. Furthermore, the wavelength range studied was rather limited and thus the emission wavelength dependence of the radiative and nonradiative rates was not fully clarified. Since almost all optical properties of Si-nc's depend strongly on the size, wavelength dependence of the rates and also the quantum efficiencies should be studied in a wider energy range starting from the band gap energy of bulk Si crystals.

In this work, we prepare $SiO_2$ films containing Si-nc's by a co-sputtering method and study the radiative and nonradiative recombination rates of Si-nc's by applying the method similar to that of Kalkman *et al.*[8] and Walters *et al.*[9] To control the PMD, we deposit a Au layer on top of the samples, and in between the Au layer and the active layer, a $SiO_2$ spacer layer with the thickness of 0–550 nm is inserted. We prepare several samples under different conditions to control the luminescence wavelength in a wide range. The wide tunability of the luminescence maximum allows us to estimate the rate and the quantum efficiency from 700 to 1100 nm, which is very close to the band gap energy of bulk Si crystals. In addition, the effects of sample preparation conditions on these parameters are obtained. We will show that the wavelength dependence of the radiative rates is on a single curve for all the samples, while the nonradiative

 

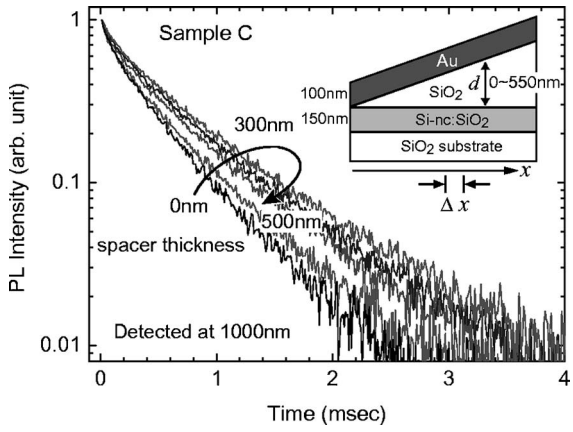


FIG. 1. PL decay curves of Si-nc's detected at 1000 nm for various spacer thicknesses (sample C). The data for the spacer thickness of 0, 200, 300, 400, and 500 nm are shown. Inset: schematic representation of the sample structure.

rates depend strongly on sample preparation conditions. We also show that the quantum efficiency is always larger at longer wavelength side.

## II. EXPERIMENTAL DETAILS

The structure of samples studied is schematically illustrated in the inset of Fig. 1. $SiO_2$ films containing Si-nc's (Si-nc's:$SiO_2$) about 150 nm in thickness are deposited on a $SiO_2$ substrate by the co-sputtering of Si and $SiO_2$, and annealed in $N_2$ gas atmosphere. Details of the procedure are described in our previous papers.[2,12] Samples with different size distributions are prepared by controlling the concentration of excess Si and the annealing temperature.[2] Sample preparation conditions and average diameters of Si-nc's are summarized in Table I. After the growth of Si-nc's by annealing, a $SiO_2$ film, which acts as a spacer between the active layer and a Au layer, is deposited by sputtering. The thickness of the spacer layer ($d$) is varied from 0 to 550 nm continuously by controlling a shutter during the sputtering. On the spacer layer, a Au film 100 nm in thickness is deposited by vacuum evaporation.

For the measurement of PL spectra and the decay curves, samples are excited by 457.9 nm light of an optical parametric oscillator (OPO) excited by the third harmonic of a neodium:yttritium-aluminum-garnet (Nd:YAG) laser through

TABLE I. Summary of sample preparation conditions. The average diameters are estimated from the PL peak wavelength versus size relation obtained previously (Ref. 2).

| Sample name | Si conc (at. %) | Annealing temp (°C) | Estimated diameter (nm) |
|---|---|---|---|
| A | 36.5 | | 3.6 |
| B | 38.6 | 1250 | 4.2 |
| C | 41.8 | | 6.0 |
| D | 41.8 | 1200 | 5.2 |

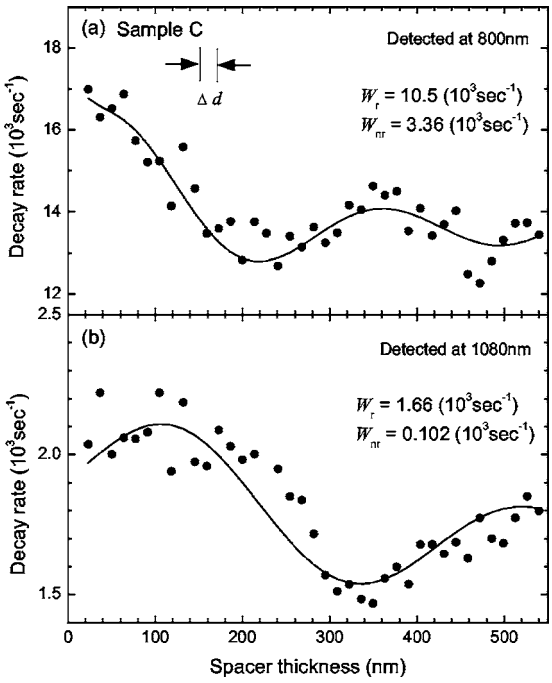


FIG. 2. PL decay rates of Si-nc's as a function of spacer thickness (closed circles) obtained at (a) 800 nm and (b) 1080 nm (sample C). Solid curves represent the results of fitting.

the transparent fuzed quartz substrates. The power, the pulse width, and the repetition frequency are 500 $\mu$J/cm$^2$, 5 ns, and 20 Hz, respectively. PL signals are collected from the same side. PL spectra are recorded by using a single grating monochromator and a liquid $N_2$ cooled InGaAs NIR diode array or a Si charge coupled device. The spectral response of the detection system is corrected with the aid of a reference spectrum of a standard tungsten lamp. For the time response measurements, a NIR photomultiplier (5509-72, Hamamatsu) and a multichannel scaler (SR430, Stanford Research) are used. The overall time resolution of the system is about 100 ns. To take the dependence of the PL decay curves on the spacer thickness, samples are mounted on a linear stage and the decay curves are measured by changing the position, i.e., the spacer thickness. In each measurement step, PL is collected from the range ($\Delta x$) of smaller than 100 $\mu$m on the surface of a sample (see the inset of Fig. 1). This corresponds to the variation of the spacer thickness ($\Delta d$) of less than 20 nm in each measurement step. All the measurements are made at room temperature.

## III. RESULTS AND DISCUSSION

Figure 1 shows PL decay curves detected at 1000 nm for sample C in Table I. The spacer thickness is changed from 0 to 550 nm. We can see that the decay curves depend strongly on the spacer thickness; as the spacer thickness increases, the decay time lengthens and shortens. To estimate the decay rate, the PL decay curves are fitted with a stretched exponential function.[15] In Fig. 2, the decay rates obtained at 800 nm [2(a)] and 1080 nm [2(b)] are plotted as a function of the spacer thickness (closed circles). Although the data are

slightly scattered, clear oscillation of the rates can be seen. In order to see whether or not the oscillation behavior depends on the excitation photon energy, we performed similar measurements by using longer wavelength light, i.e., 488, 510, and 560 nm, as excitation sources. The results obtained were nearly independent of the excitation photon energy.

To quantitatively analyze the oscillation behavior of the PL decay rates, we calculate the normalized decay rates of Si-nc's $[\Gamma(d,\lambda)]$ by the procedure reported previously,[16–18] where $\lambda$ is the wavelength. In the calculation, emitters are treated as an isotropic dipole positioned at a distance from the metal or dielectric surface in an arbitrary medium. The dipole field interferes with the field reflected by the surface, and the interference modifies the radiative rate of the dipole. In addition, when the dipole field couples to the surface plasmon polariton modes or lossy surface wave modes in metal, nonradiative energy transfer from the dipole to the modes occurs, which results in the increase of the decay rate.[8,18]

For practical calculation the samples are modeled as a four layer system as shown in the inset of Fig. 1.[19] To obtain decay rates of an isotropic dipole, the calculated results are averaged over polarization. Furthermore, since the actual samples have a finite thickness, the decay rates of emitters positioned at different depths are convoluted over the thickness of the active layer (150 nm). The dielectric constants of Au, Si, and $SiO_2$ are taken from Ref. 20, and that of the active layer is estimated by the Bruggeman effective medium theory.[21] The dielectric constants of the active layer used for the calculation for samples A, B, C, and D are 2.19, 2.28, 2.37, and 2.37, respectively. The dispersion of the dielectric constant of Au is considered, while those of Si and $SiO_2$ are not taken into account because they do not strongly affect the calculated results in the wavelength range studied.

In the following, we estimate radiative $[W_r(\lambda)]$ and nonradiative $[W_{nr}(\lambda)]$ decay rates of Si-nc's by the procedure proposed by Kalkman *et al.*[8] and Walters *et al.*[9] If the internal quantum efficiency of Si-nc's is 100%, the spacer thickness dependence of the decay rate obtained experimentally $[W_{exp}(d,\lambda)]$ is proportional to that of calculated normalized decay rate $[\Gamma(d,\lambda)]$. On the other hand, if there are nonradiative processes, it is not proportional to $\Gamma(d,\lambda)$. Under the assumption that the nonradiative rate is not modified by PMD, the measured decay rate is expressed as[22–25]

$$W_{exp}(d,\lambda) = W_r(\lambda)\cdot\Gamma(d,\lambda) + W_{nr}(\lambda). \quad (1)$$

This equation means that the amplitude of the oscillation of the decay rate with respect to the total rate becomes smaller with increasing $W_{nr}(\lambda)$, i.e., with decreasing the quantum efficiency. By fitting Eq. (1) to experimental data, $W_r(\lambda)$ and $W_{nr}(\lambda)$ are obtained independently.

It is worth noting here that in actual samples light collection efficiency depends on the distance from the metal layer. In the very short distance range (~10 nm) from the metal layer, the collection efficiency is very small because of the efficient nonradiative energy transfer from the emitter to the lossy surface wave modes in the metal.[8] In this range, the calculated decay rates are very large, but we do not observe the large increase of the decay rate when the spacer thickness approaches zero. This is because PL arises mainly from the lower part of the active layer (150 nm in thickness), where the interaction with the lossy modes is negligible. In the middle distance (~70 nm), the rate of the energy transfer from the emitter to the surface plasmon polariton modes is larger than the radiative rate,[8] and thus the collection efficiency depends also on the distance from the metal, although the dependency is much smaller than the short distance range. In the distance larger than ~70 nm, the radiative recombination is the major recombination process, and thus the distance dependence of the collection efficiency becomes small. Therefore, in most of the spacer thickness range studied, the distance dependence of the collection efficiency is considered to be very small and thus does not significantly affect the values of $W_r(\lambda)$ and $W_{nr}(\lambda)$ estimated by the fitting procedure.

In Fig. 2, the results of the fitting (solid curves) are shown for two different detection wavelengths for sample C. Although the data are scattered, the agreement is satisfactory. The values of $W_r(\lambda)$ and $W_{nr}(\lambda)$ obtained by the fittings are given in the figures. To discuss the wavelength dependence of the decay rates we performed the fitting procedure for all the samples at different wavelengths. In Fig. 3(a) the estimated radiative decay rates are plotted as a function of the wavelength for sample A (closed squares), B (closed circles), C (triangles), and D (inverted triangles). We can see that all the data obtained for four samples prepared under different conditions are on a single curve. The coincidence of the radiative decay rates for all the samples in a wide wavelength range supports the validity of the present procedure. Furthermore, the coincidence implies that the radiative rate is determined only by the size of nanocrystals and is immune to the difference in the local structures arising from different sample preparation conditions. The radiative rate increases as the emission wavelength decreases, i.e., as the size becomes smaller. This is mainly due to larger overlap of electron and hole wave functions in the momentum space by the quantum confinement effect.[26]

In Eq. (1), the nonradiative rate is assumed not to be modified by PMD. If the nonradiative rate is modified by PMD, the experimentally obtained oscillation would not be fitted by Eq. (1). Even if the fitting is possible accidentally, the values of $W_r$ and $W_{nr}$ may not be correct, and $W_r$ would not be on a sample-independent single curve. Therefore, the coincidence of the estimated radiative rates for all the samples [Fig. 3(a)] is evidence that the assumption is appropriate.

In contrast to the radiative rate, the nonradiative rate depends strongly on samples. In Fig. 3(b), wavelength dependence of the nonradiative decay rates is plotted. Although all the data show similar wavelength dependence, i.e., the nonradiative rate increases as the wavelength becomes shorter, the values are strongly dependent on samples. The nonradiative rate is larger for samples with higher excess Si concentration and annealed at lower temperatures.

In Fig. 3(c), the internal quantum efficiencies $[\eta = W_r/(W_r + W_{nr})]$ are plotted as a function of the wavelength. Because of the strong sample dependence of the nonradiative rate, the quantum efficiency also depends strongly on samples. If we compare the quantum efficiency at the

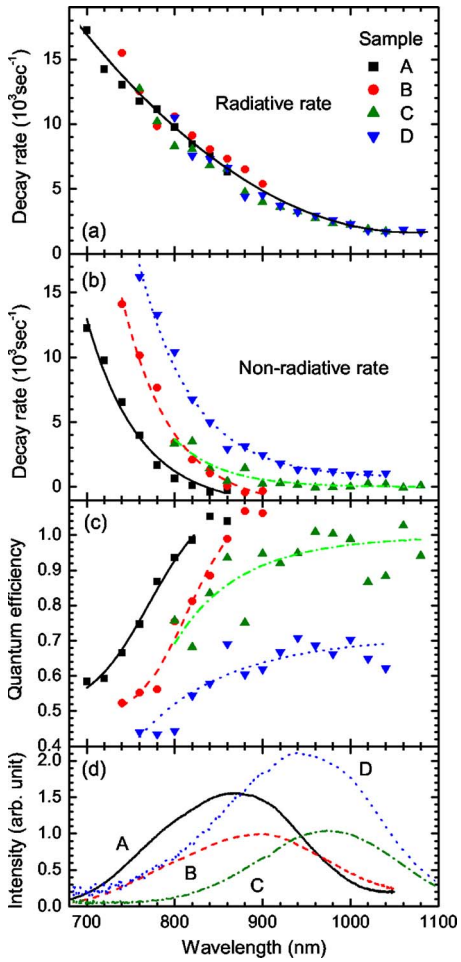


FIG. 3. (Color online) (a) Radiative decay rates, (b) nonradiative decay rates, and (c) PL quantum efficiencies of samples A (closed squares), B (closed circles), C (triangles), and D (inverted triangles) as a function of wavelength. (d) PL spectra of samples A (solid curve), B (dashed curve), C (dashed-dotted curve), and D (dotted curve).

same wavelength, it is larger for the samples containing smaller amounts of excess Si and annealed at higher temperatures. For all the samples, the quantum efficiency is larger at longer wavelength, i.e., for larger nanocrystals in size distribution. For the samples annealed at 1250 °C (samples A, B, and C), the quantum efficiency is close to 100%, while that annealed at 1200 °C (sample D), the maximum efficiency is about 70%.

The quantum efficiencies estimated in this work are apparently larger than the total quantum efficiency of Si-nc assemblies reported previously (external quantum efficiency ~ several percent,[5–7] internal quantum efficiency <10%[7]). This discrepancy implies that there are a lot of Si-nc's which do not contribute to PL. In Fig. 3(c), at the larger side of the size distribution of samples A, B, and C, the quantum efficiency is close to 100%. Therefore, in these samples at the larger side of the size distribution, Si-nc's can be classified into two categories; "bright" Si-nc's with the quantum efficiency of 100% and "dark" Si-nc's with that of 0%. In dark Si-nc's, the rate of nonradiative recombination processes is much larger than the radiative rate and thus these Si-nc's do not contribute to PL at all. The total quantum efficiency is determined simply by the number ratio of the bright and dark Si nanocrystals. At the smaller side of the size distribution of samples A, B and C, and in the whole size distribution range of sample D, the quantum efficiency of bright nanocrystals is less than 100%. Quantum efficiency smaller than 100% implies that in addition to very efficient nonradiative processes, which completely kill PL of a nanocrystal, relatively slow nonradiative recombination processes, the rate of which is comparable to the radiative rate, exist in these Si-nc's.

It is possible that defects at or near Si-$SiO_2$ interfaces are responsible for the slow nonradiative process, although microscopic structures of the defects are not identified. The other possible origin of the slow nonradiative process is the Förster type energy transfer from small to large nanocrystals.[10] The probability of this process is larger for smaller nanocrystals in size distribution because of larger probability of finding nanocrystals with smaller band gap energies nearby. Therefore, the nonradiative rate is larger for smaller nanocrystals, i.e., at the shorter wavelength side of PL bands. This is consistent with the results in Fig. 3(b). In Fig. 3(b), the nonradiative rates are larger for the samples containing larger amount of excess Si. This can also be explained by the model because the increase in the amount of Si results in the decrease in the average separation between Si-nc's and larger rates of the Förster process. However, this model is not enough to explain all the data. If only this process is the origin of the slow nonradiative process, the quantum efficiency should always reach 100% at the lower energy side of the PL band. However, as can be seen in Fig. 3(c), for the sample annealed at 1200 °C it is saturated at 70%. Therefore, some different processes are considered to be responsible for the slow nonradiative process.

Recently, there has been a controversy whether or not the rate of Förster type energy transfer is modified by PMD. Dood *et al.* demonstrated that energy transfer between Er ions in glasses is not modified by PMD,[25] while Barnes showed that energy transfer between different kinds of molecules is modified.[27] In our previous work,[19] we showed that the rate of energy transfer from Si-nc's to Er ions is modified by PMD, although the mechanism of the energy transfer was not clarified. As discussed above, the present results strongly suggest that nonradiative rates in Si-nc's are not modified by PMD. Therefore, if the slow nonradiative process is (at least partly) due to the Förster energy transfer between nanocrystals, the present result provides the evidence that the energy transfer rate is not modified by PMD. However, at present we have no definite evidence of energy transfer between nanocrystals, and thus cannot conclude definitely.

It is worth noting that the higher quantum efficiency of individual nanocrystals comprising the samples does not always result in the higher total quantum efficiency of the sample. In Fig. 3(d), the PL intensity is the largest for sample D in a wide wavelength range, despite the lower quantum efficiency of bright nanocrystals in sample D (<70%) than those in other samples. This supports the above conclusion that the main factor which determines the total quantum efficiency of samples is not a quantum efficiency of individual nanocrystals but the number of bright nanocrystals.

## IV. CONCLUSION

Radiative and nonradiative recombination rates of excitons confined in Si nanocrystals are estimated independently. It is found that the radiative rates obtained for four samples prepared under different conditions agree very well and are on a single radiative-rate versus wavelength curve. This result implies that the radiative recombination rate of excitons in oxygen terminated Si-nc's is determined only by the size of Si-nc's and is immune to sample preparation conditions. It is of great interest to compare the present results with the radiative rate of hydrogen terminated Si-nc's.

In contrast to the radiative rate, the nonradiative rate depends strongly on sample preparation conditions. The nonradiative rate is smaller for the samples annealed at higher temperatures and containing smaller amount of excess Si. For the samples annealed at 1250 °C, the estimated internal quantum efficiency is close to 100% at longer wavelength side of the PL bands, while it is saturated at 70% for that annealed at 1200 °C. The high quantum efficiency obtained indicates that, in Si nanocrystal assemblies, the majority of nanocrystals in samples do not contribute to PL and a small number of nanocrystals luminesce with a high quantum efficiency, resulting in a rather small total quantum efficiency.

## ACKNOWLEDGMENT

This work is supported by a Grant-in-Aid for Scientific Research from the Ministry of Education, Culture, Sports, Science and Technology, Japan.

*Author to whom correspondence should be addressed; electronic address; fujii@eedept.kobe-u.ac.jp

[1] L. T. Canham, Appl. Phys. Lett. **57**, 1046 (1990).
[2] S. Takeoka, M. Fujii, and S. Hayashi, Phys. Rev. B **62**, 16820 (2000).
[3] C. Delerue, M. Lannoo, G. Allan, and E. Martin, Thin Solid Films **255**, 27 (1995).
[4] D. Kovalev, H. Heckler, G. Polisski, and F. Koch, Phys. Status Solidi B **215**, 871 (1999).
[5] W. L. Wilson, P. F. Szajowski, and L. E. Brus, Science **262**, 1242 (1994).
[6] J. C. Vial, A. Bsiesy, F. Gaspard, R. Hérino, M. Ligeon, F. Muller, R. Romestain, and R. M. Macfarlane, Phys. Rev. B **45**, 14171 (1992).
[7] V. A. Skryshevsky, A. Laugier, V. I. Strikha, and V. A. Vikulov, Mater. Sci. Eng., B **40**, 54 (1996).
[8] J. Kalkman, H. Gersen, L. Kuipers, and A. Polman, Phys. Rev. B **73**, 075317 (2006).
[9] R. J. Walters, J. Kalkman, A. Polman, H. A. Atwater, and M. J. A. de Dood, Phys. Rev. B **73**, 132302 (2006).
[10] F. Priolo, G. Franzó, D. Pacifici, V. Vinciguerra, F. Iacona, and A. Irrera, J. Appl. Phys. **89**, 264 (2001).
[11] D. Cha, J. H. Shin, I. H. Song, and M. K. Han, Appl. Phys. Lett. **84**, 1287 (2004).
[12] Y. Kanzawa, T. Kageyama, S. Takeoka, M. Fujii, S. Hayashi, and K. Yamamoto, Solid State Commun. **102**, 533 (1997).
[13] L. Tsybeskov, K. D. Hirschman, S. P. Duttagupta, M. Zacharias, P. M. Fauchet, J. P. McCaffrey, and D. J. Lockwood, Appl. Phys. Lett. **72**, 43 (1998).
[14] M. Zacharias, J. Heitmann, R. Scholz, U. Kahler, M. Schmidt, and J. Bläsing, Appl. Phys. Lett. **80**, 661 (2002).
[15] G. Mauckner, K. Thonke, T. Baier, T. Walter, and R. Sauer, J. Appl. Phys. **75**, 4167 (1994).
[16] K. H. Drexhage, in *Progress in Optics XII*, edited by E. Wolf (North-Holland, Amsterdam, 1974), p. 165.
[17] R. R. Chance, A. Prock, and R. Silbey, Adv. Chem. Phys. **37**, 1 (1978).
[18] W. L. Barnes, J. Mod. Opt. **45**, 661 (1998).
[19] T. Nakamura, M. Fujii, K. Imakita, and S. Hayashi, Phys. Rev. B **72**, 235412 (2005).
[20] D. W. Lynch and W. R. Hunter, *Handbook of Optical Constants of Solid*, edited by E. D. Palik (Academic, New York, 1985).
[21] P. A. Snow, E. K. Squire, P. St. J. Russell, and L. T. Canham, J. Appl. Phys. **86**, 1781 (1999).
[22] E. Snoeks, A. Lagendijk, and A. Polman, Phys. Rev. Lett. **74**, 2459 (1995).
[23] T. M. Hensen, M. J. A. de Dood, and A. Polman, J. Appl. Phys. **88**, 5142 (2000).
[24] M. J. A. de Dood, L. H. Slooff, A. Polman, A. Moroz, and A. van Blaaderen, Phys. Rev. A **64**, 033807 (2001).
[25] M. J. A. de Dood, J. Knoester, A. Tip, and A. Polman, Phys. Rev. B **71**, 115102 (2005).
[26] T. Takagahara and K. Takeda, Phys. Rev. B **46**, 15578 (1992).
[27] P. Andrew and W. L. Barnes, Science **290**, 785 (2000).